Exploring the electronic properties and oxygen vacancy formation in $SrTiO_3$ under strain

Lan, Zhenyun; Vegge, Tejs; Castelli, Ivano E.

Published in:
Computational Materials Science

Link to article, DOI:
10.1016/j.commatsci.2023.112623

Publication date:
2024

Document Version
Publisher's PDF, also known as Version of record

Computational Materials Science 231 (2024) 112623

Contents lists available at ScienceDirect

Computational Materials Science

journal homepage: www.elsevier.com/locate/commatsci

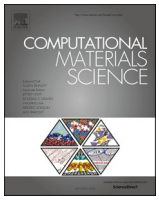

Full Length Article

Exploring the electronic properties and oxygen vacancy formation in $SrTiO_3$ under strain

Zhenyun Lan [a,b], Tejs Vegge [a], Ivano E. Castelli [a,*]

[a] Department of Energy Conversion and Storage, Technical University of Denmark, Anker Engelundsvej 411, DK-2800 Kgs. Lyngby, Denmark
[b] School of Materials Science and Engineering, Hefei University of Technology, Hefei, Anhui 230009, PR China

ARTICLE INFO

Keywords:
DFT calculations
$SrTiO_3$
Electronic properties
Oxygen vacancy
Strain

ABSTRACT

$SrTiO_3$ (STO) thin films are widely used as substrates in oxide-based devices, and although STO is one of the most studied materials, both experimentally and computationally in its bulk form, the potential for strain engineering of STO thin-films is largely ignored. In this work, we perform Density Functional Theory (DFT) calculations to investigate the tuning of the structural and electronic properties of STO thin films under uni- and biaxial strain. We find that for TiO_2-terminated STO slab, the band gap changes due to strain are more significant than that of the SrO-terminated surface because the band gap is determined by the TiO_2 layers closer to the surface. Furthermore, we also find that the formation energy of oxygen vacancies depends on the type of strain applied and the position of oxygen vacancies. These findings demonstrate the large and hitherto underexplored perspectives of using strain engineering to modulate the structural and electronic properties of perovskite film materials for a wide variety of energy and electronic applications.

1. Introduction

Strontium titanate ($SrTiO_3$, STO), one of the most studied perovskites, is a material with unique physical properties, such as the photocatalytic ability for water splitting [1,2], strain-induced ferroelectricity [3,4], and a two-dimensional electron gas behavior [5,6], which make STO widely used in several devices, both as active material and substrate. Moreover, the electronic structure properties of STO can be adjusted by modifying its crystal structure. Temperature effects, synthesis conditions, defects, and external parameters, such as strain, directly affect the materials' properties [7] and make the phase space of STO complex and interesting for various applications.

STO can be fabricated in many forms, from thick substrate to thin films [8,9], as well as it can be manipulated by adding strain, e.g., by using polymeric support, a three-point bending apparatus [10], or induced by epitaxial growth [11]. Despite this, a systematic study of the effect that uniaxial and biaxial strain have on the structural and electronic properties of thin-films of STO is currently uncharted territory and is the focus of this work.

In the most controlled form, strain engineering can be efficiently used to modulate the crystal structure as a pathway to control the physical properties of materials, from electronic to catalytic [12–15]. For instance, first-principle study shows that strain drives phase transition in incipient ferroelectric STO [16]. The optical band gap of the prototypical semiconducting oxide, SnO_2, can be continuously controlled by single-axis lattice strain [17]. In the case of STO, a comprehensive investigation has been carried out to study the effects of strain on the thermoelectric properties of STO [18]. It has been reported that the electron mobility of STO films can be enhanced by strain [19]. Although these examples consider the materials in their bulk (3D) form, the interface is often the key to obtaining new, unique properties [7]. As an example, compared to biaxial strain, uniaxial strain significantly changes the crystal structure because of a breaking of the symmetry, followed by exciting properties such as band splitting in thin films STO [20]. Our previous work has demonstrated that strain engineering can enhance the performance of the oxygen evolution reaction (OER) on the surface of metal oxynitride $BaTaO_2N$ materials for water splitting [21]. Furthermore, we can imagine situations where strain can be dynamically adjusted during electrocatalytic reactions, thus tuning the energetics of the reaction intermediates and achieving almost loss-less reaction pathways, as shown for $InSnO_2N$ [22,23]. Studies also show that uniaxial strain can turn the band gap of the 2D monolayer $MoSe_2$ [24], and induce a giant anisotropic Raman response of encapsulated ultrathin black phosphorus [25]. Furthermore, reports have shown that

* Corresponding author.
E-mail address: ivca@dtu.dk (I.E. Castelli).

https://doi.org/10.1016/j.commatsci.2023.112623
Received 25 July 2023; Received in revised form 27 October 2023; Accepted 27 October 2023
Available online 2 November 2023

strain can manipulate the formation of oxygen vacancies, which often spontaneously occur during the synthesis process and are one of the pathways in tailoring the properties of materials, from magnetic and electronic to the formation of a two-dimensional electron gases (2DEG) [26–31].

In this work, we investigate both structural and electronic properties of STO under uniaxial and biaxial strains, e.g., elucidating the changes in the formation of oxygen vacancies and changes in the band gap, which is a common descriptor for solar cells and water splitting devices, photodetectors, and light-emitting diodes (LEDs) [32].

2. Method

All calculations were performed in the framework of DFT using the strongly constrained and appropriately normed (SCAN) *meta*-GGA exchange correlation functional [33] as implemented in the Vienna ab-initio simulation package (VASP) [34]. SCAN functionals can, in many cases, yield an accuracy comparable to hybrid GGAs, almost at the cost of a GGA calculation and without a Hubbard U correction [34–36]. We note that although the electronic occupation is calculated correctly using SCAN, the band gap values are still underestimated. Despite this, our conclusions are solid and will not change by using more accurate, although computationally prohibitive for our model calculations. The Brillouin zone was sampled with a 4x4x1 Γ–centered k-point grid for the studied configurations. A plane wave cutoff of 700 eV was used for the optimization of the structure with oxygen vacancies. For the bulk structure, the energy cutoff was set as 875 eV. The structures were optimized until the force on each atom was less than 0.03 eV/Å. Our model systems were obtained by repeating the cubic structure of STO 2x2x5.5 times, corresponding to a STO structure oriented in the [0 0 1] direction with both TiO_2/SrO-terminations. To find the relaxed configuration of the unstrained slab, we have optimized the value of a and b lattice parameters while constraining c, which is the direction orthogonal to the slab surface. All atomic positions are fully relaxed. This slab model is the starting point for the strained cases, where strain has been added to the a and/or b lattice parameters. After full relaxation, the cubic symmetry of the slab could be broken. All the structures and outputs of the calculations are stored and freely available in the DTU DATA repository (https://doi.org/10.11583/DTU.20036264) [37].

The O vacancy formation energy is defined as

$$E_O = E_{removed} - E_{slab} + \mu_O$$

where $E_{removed}$ is the energy of the slab with defects and E_{slab} is the energy of the slab. μ_O is the chemical potential of the O that is removed. The chemical potential of the O is referenced to O_2 gas from H_2O and H_2 gas.

3. Result and discussion

As a starting point, we consider the cubic structure, with the space group Pm $\overline{3}$ m, as this phase is a typical representative of bulk STO at room temperature. The optimized lattice constant of bulk STO (Fig. 1 a) is a = 3.906 Å, which agrees well with experimental results (a = 3.906 Å) [38]. Cleaving bulk STO in [0 0 1] direction, 2 × 2 × 5.5 STO slabs with two TiO_2 or SrO terminations are built, as shown in Fig. 1 b and c, respectively. The lattice constant for the optimized STO slab is a = b = 3.886 Å, which is slightly smaller than the bulk value. This is, however, in good agreement with previous literature [39].

The effect of epitaxial strain on the band gap of the STO slab is investigated. From Fig. 2, we can see that the band gap of the TiO_2-terminated STO slab changes under uni/bi-axial strain. Under tensile strain, the band gap of the TiO_2-terminated STO slab increases monotonically for both uniaxial and biaxial strains. And under tensile biaxial strain, the band gap changes more significantly than under tensile uniaxial strain. However, the responses to the compressive strain are different. Applying the compressive uniaxial strain slightly increases the

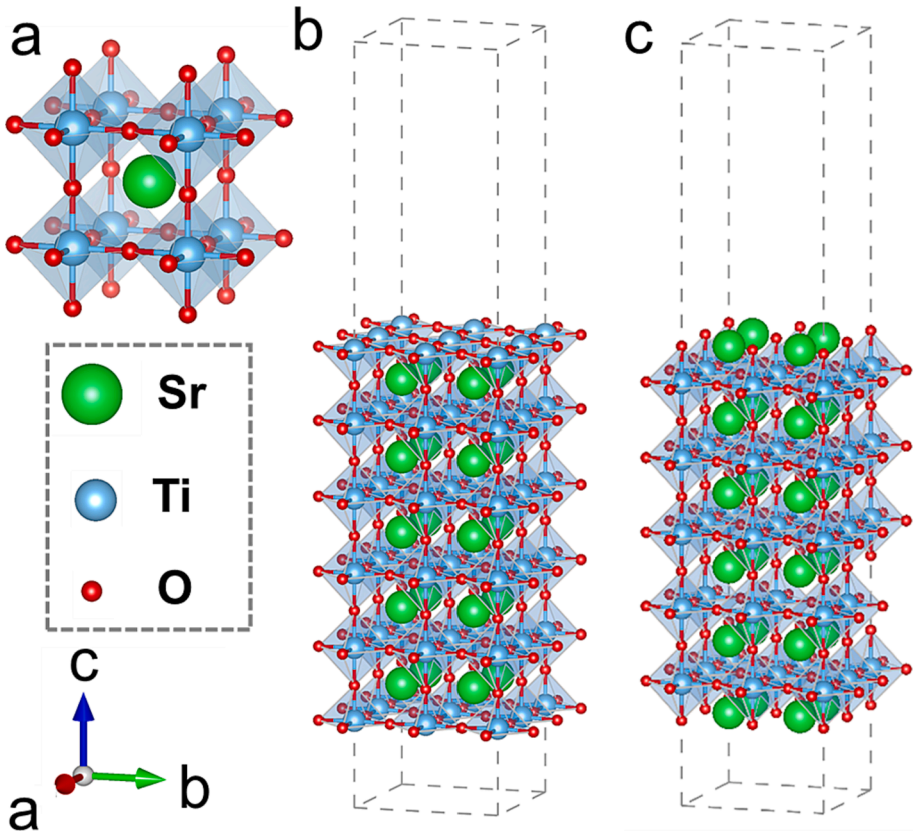

Fig. 1. Structures of (a) bulk STO, (b) TiO_2-terminated, and (c) SrO-terminated STO slab.

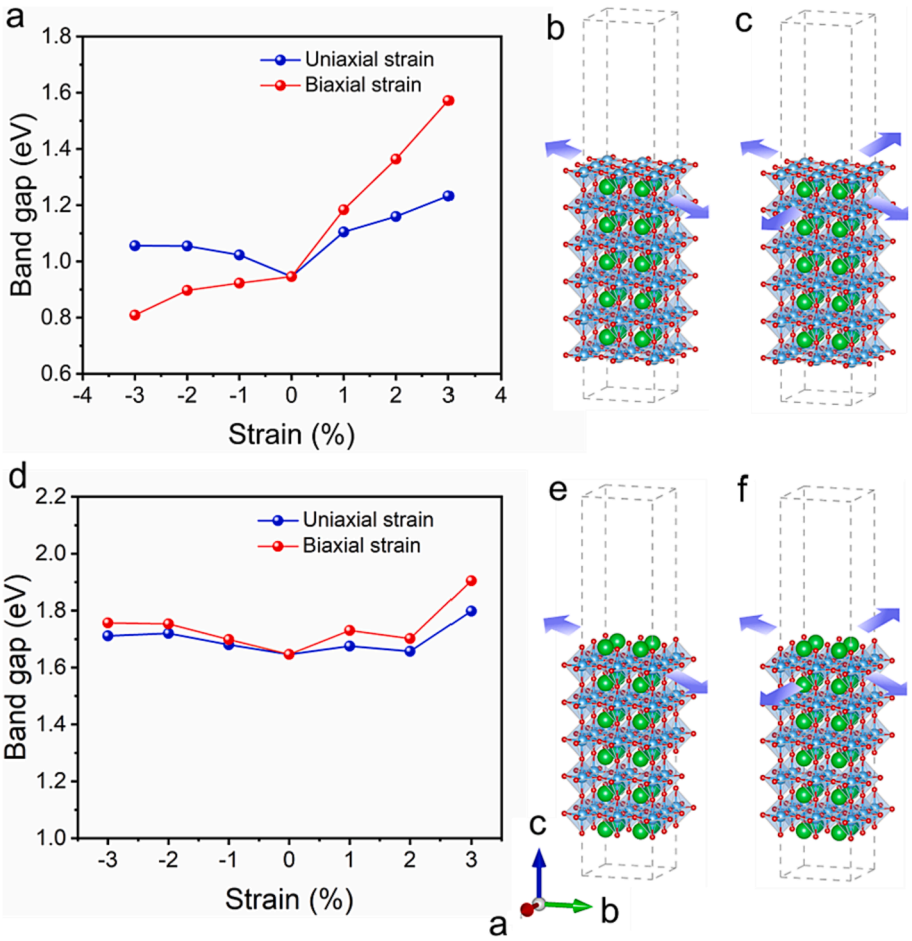

Fig. 2. The band gap of (a) TiO_2-terminated and (d) SrO-terminated STO slab as a function of strain.Schematic of TiO_2-terminated STO slab under (b) uniaxial and (c) biaxial strain. Schematic of SrO-terminated STO slab under (e) uniaxial and (f) biaxial strain.

band gap of the TiO_2-terminated STO slab. When the compressive biaxial strain is applied, the band gap of the TiO_2-terminated STO slab decreases. For the SrO-terminated slab, the band gap changes similarly under both uniaxial and biaxial strain. Under compressive stain, the band gap almost keeps the same. At 3 % tensile strain, the band gap has an apparent increase.

The band gap change for the TiO_2-terminated STO slab is more significant, which can be explained by the layer-resolved PDOS figure in Fig. 3b and f. The band gap is determined by the TiO_2 surface layers for the TiO_2-terminated STO slab, while the TiO_2 layer influences the band gap in the second layer for the SrO-terminated STO slab. When the strain is applied, the structure of the surface layers changes more significantly than the inner layer, resulting in a more significant change of band gap for the STO slab with TiO_2 terminations.

Besides strain, oxygen vacancies also influence electronic properties. The poor oxygen condition or reduction environment can drive the formation of oxygen vacancies [40]. In addition, the strain has been reported to further influence the formation of oxygen vacancies [30,31]. As shown in Fig. 3, for TiO_2-terminated slabs, the vacancy states tend to be delocalized when the oxygen vacancies are on the surface (Fig. 3b). The formation energy of oxygen vacancies on the surface is more negative than the formation energy of oxygen vacancies on the subsurface, so the oxygen vacancies prefer to be located on the surface instead of the subsurface. We can observe that vacancy states are localized at the surface and subsurface of the slab when the oxygen vacancies are in the subsurface (Fig. 3d). For the SrO-terminated slab, it is also energetically more favorable to have oxygen vacancies on the surface. When oxygen vacancies are on the surface, the localization of vacancies states exists on the surface, which can result in a 2DEG on the surface. When the oxygen vacancies are on the subsurface of the SrO-terminated slab, the vacancy states tend to be delocalized (Fig. 3f). Therefore, the vacancy states are localized for both TiO_2 and SrO terminated slabs when the oxygen vacancies are in the SrO layer.

To further control the electronic properties of the STO slab, we investigate the strain engineering effects on the formation of oxygen vacancies. When the oxygen vacancies are on the surface of the TiO_2-terminated slab (Fig. 4a), their formation energy increases with the compressive uniaxial strain while decreasing with the tensile strain. However, when biaxial strain is applied, the formation energy of surface oxygen vacancies changes differently. Under compressive strain, the formation energy decreases, increases slightly, and decreases again. While under tensile strain, the formation energy decreases slightly and increases with strain. For the oxygen vacancies in the sublayer, the formation energy of oxygen vacancies increases slowly under compressive uniaxial strain. Still, it increases gradually under tensile uniaxial strain, as shown in Fig. 4b. Under biaxial strain, when the slab is compressed, the formation energy of these oxygen vacancies decreases. At the same time, it increases when 1 % tensile strain is applied and then keeps almost the same when the strain is increased for the SrO-terminated slab; when the oxygen vacancies on the surface (Fig. 4c), with compressive uniaxial strain, the formation energy is same under 1 % compressive strain and decreases when the strain increases. When we stretch the slab, the formation energy of oxygen vacancies on the surface decreases at first and increases after a 2 % tensile strain is applied. When applying biaxial strain, the formation energy increases under compressive strain and decreases under tensile strain. For the oxygen vacancies

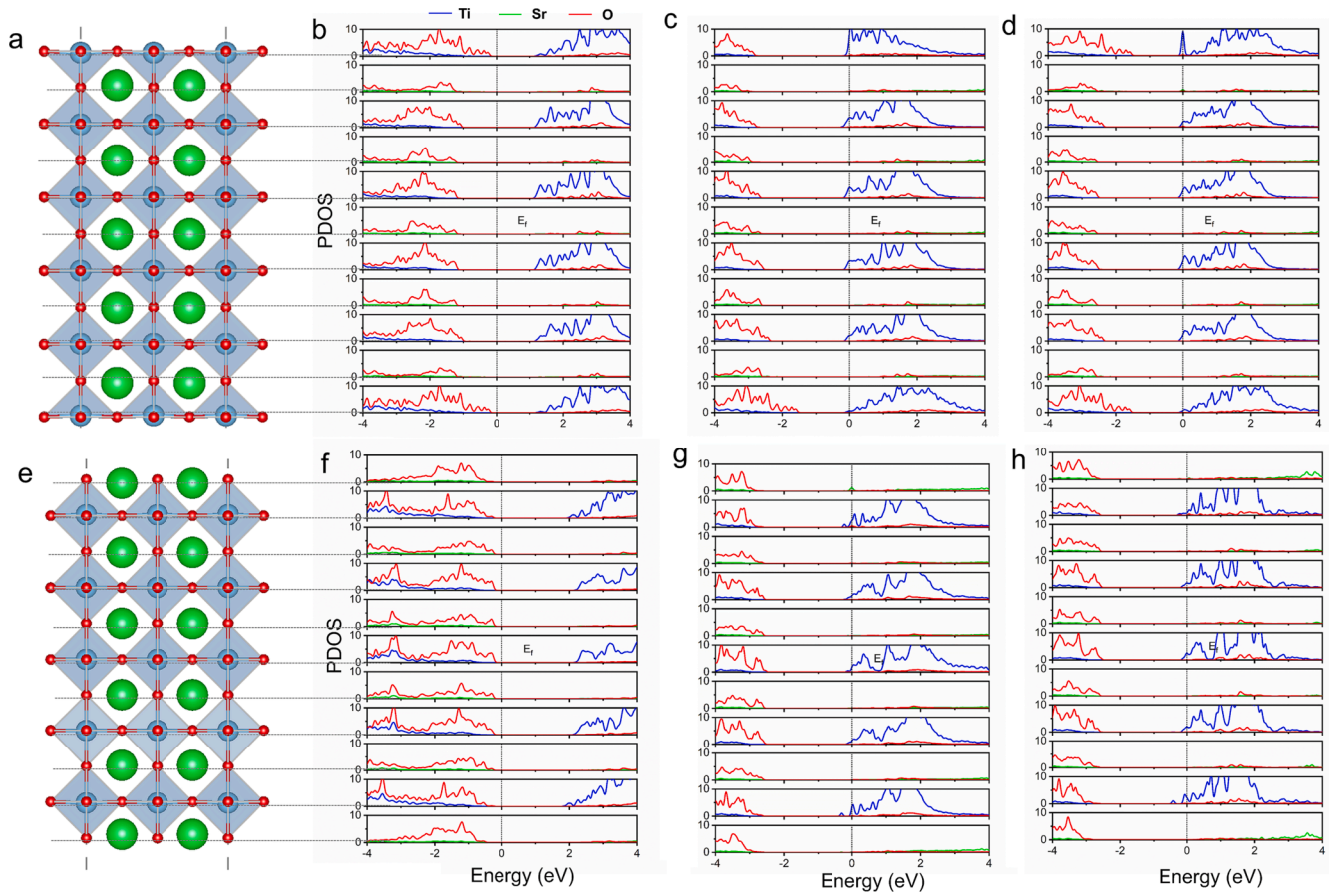

Fig. 3. (a) Side view of TiO_2-terminated STO slab. Layer-resolved partial density of states (PDOS) of TiO_2-terminated STO slab (b) without oxygen vacancies, with (c) oxygen vacancies on the surface and (d) in the sublayer. (e) Side view of SrO-terminated STO slab. Layer-resolved PDOS of SrO-terminated STO slab (f) without oxygen vacancies, with (g) oxygen vacancies on the surface and (h) in the sublayer.

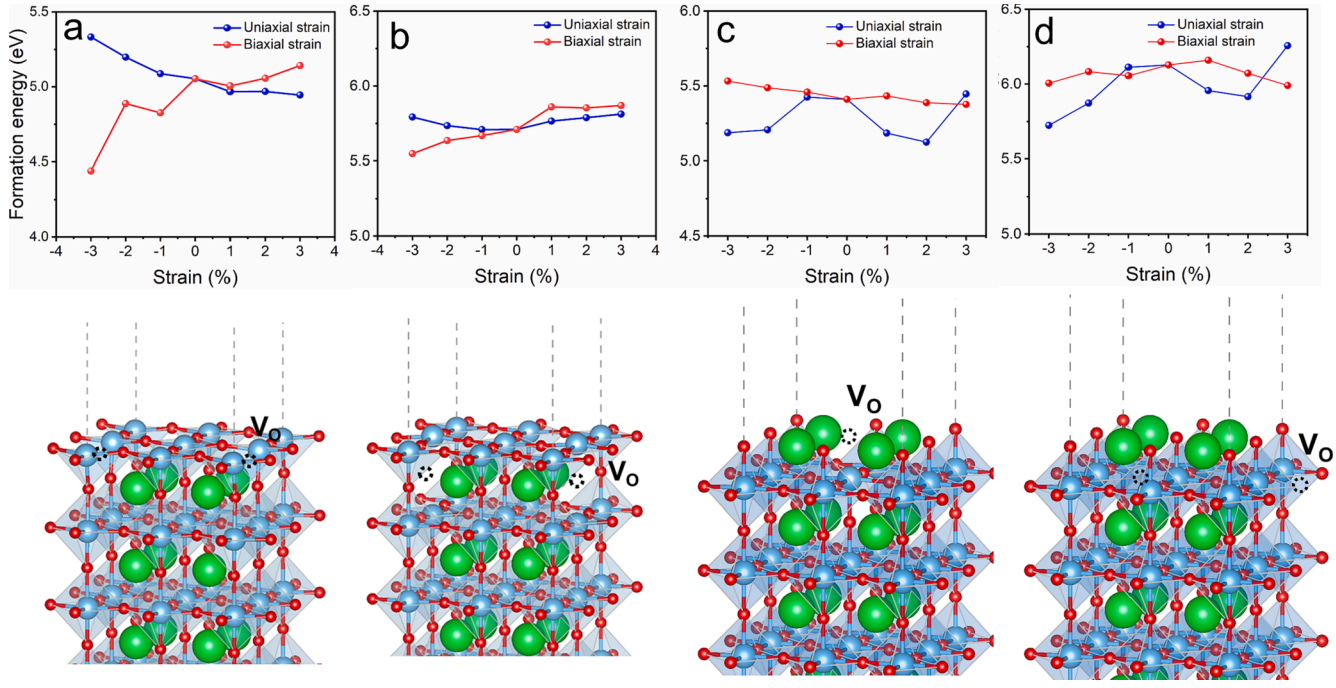

Fig. 4. The formation energy of oxygen vacancies under strain for TiO_2-terminated STO slab with (a) oxygen vacancies on the surface and (b) in the sublayer, respectively. The formation energy of oxygen vacancies under strain for SrO-terminated STO slab with (c) oxygen vacancies on the surface and (d) in the sublayer, respectively.

in the sublayer (Fig. 4d), under uniaxial strain, the changing trend of formation energy of oxygen vacancies is the same as the oxygen vacancies on the surface. When applying compressive strain under biaxial strain, oxygen vacancies' formation energy in the sublayer decreases, then increases a little and decreases again; using tensile strain, it increases first and then decreases. The strain influence on the formation energy of oxygen vacancies thus depends on the type of strain applied and the position of oxygen vacancies.

4. Conclusion

DFT calculations have been performed to study the electronic properties of the STO slab. We have shown the effect of strain and oxygen vacancies on electronic properties. Biaxial strain will significantly change the TiO_2-terminated STO slab's band gap. When oxygen vacancies on the surface for both TiO_2-terminated and SrO-terminated slab, there exist local states. Additionally, we have found that strain effects on oxygen vacancy formation are related to the vacancy position and type of strain. These results could serve as guiding principles in the application of STO slabs in strained systems.

CRediT authorship contribution statement

Zhenyun Lan: Methodology, Formal analysis, Investigation, Writing – original draft. **Tejs Vegge:** Conceptualization, Supervision, Resources, Writing – review & editing. **Ivano E. Castelli:** Conceptualization, Supervision, Funding acquisition, Methodology, Writing – review & editing.

Declaration of competing interest

The authors declare that they have no known competing financial interests or personal relationships that could have appeared to influence the work reported in this paper.

Data availability

All the structures and outputs of the calculations are stored and freely available in the DTU DATA repository (DOI: 10.11583/DTU.20036264).

Acknowledgement

Z. L. acknowledges support from the Villum Foundation (no. 50242).

References

[1] B. Wang, S. Shen, L. Guo, Surface reconstruction of facet-functionalized $SrTiO_3$ nanocrystals for photocatalytic hydrogen evolution, ChemCatChem 8 (2016) 798–804, https://doi.org/10.1002/cctc.201501162.
[2] K. Iwashina, A. Kudo, Rh-doped $SrTiO_3$ photocatalyst electrode showing cathodic photocurrent for water splitting under visible-light irradiation, J. Am. Chem. Soc. 133 (2011) 13272–13275, https://doi.org/10.1021/ja2050315.
[3] A. Verma, S. Raghavan, S. Stemmer, D. Jena, Ferroelectric transition in compressively strained $SrTiO_3$ thin films, Appl. Phys. Lett. 107 (2015), https://doi.org/10.1063/1.4935592.
[4] R. Wördenweber, E. Hollmann, R. Kutzner, J. Schubert, Induced ferroelectricity in strained epitaxial $SrTiO_3$ films on various substrates, J. Appl. Phys. 102 (2007), https://doi.org/10.1063/1.2773680.
[5] S.M.K. Walker, F.Y. Bruno, Z. Wang, A. De La Torre, S. Riccó, A. Tamai, T.K. Kim, M. Hoesch, M. Shi, M.S. Bahramy, P.D.C. King, F. Baumberger, Carrier-density control of the $SrTiO_3$ (001) surface 2D electron gas studied by ARPES, Adv. Mater. 27 (2015) 3894–3899, https://doi.org/10.1002/adma.201501556.
[6] P. Delugas, V. Fiorentini, A. Mattoni, A. Filippetti, Intrinsic origin of two-dimensional electron gas at the (001) surface of $SrTiO_3$, Phys. Rev. B – Condensed Matter Mater. Phys. 91 (2015), https://doi.org/10.1103/PhysRevB.91.115315.
[7] V. Esposito, I.E. Castelli, Metastability at defective metal oxide interfaces and nanoconfined structures, Adv. Mater. Interfaces 7 (2020) 1902090, https://doi.org/10.1002/admi.201902090.
[8] H.W. Jang, A. Kumar, S. Denev, M.D. Biegalski, P. Maksymovych, C.W. Bark, C. T. Nelson, C.M. Folkman, S.H. Baek, N. Balke, C.M. Brooks, D.A. Tenne, D. G. Schlom, L.Q. Chen, X.Q. Pan, S.V. Kalinin, V. Gopalan, C.B. Eom, Ferroelectricity in strain-free $SrTiO_3$ thin films, Phys. Rev. Lett. 104 (2010), 197601, https://doi.org/10.1103/PhysRevLett.104.197601.
[9] M.D. McDaniel, T.Q. Ngo, A. Posadas, C. Hu, S. Lu, D.J. Smith, E.T. Yu, A. A. Demkov, J.G. Ekerdt, A chemical route to monolithic integration of crystalline oxides on semiconductors, Adv. Mater. Interfaces 1 (2014) 1400081, https://doi.org/10.1002/admi.201400081.
[10] B. Jalan, S.J. Allen, G.E. Beltz, P. Moetakef, S. Stemmer, Enhancing the electron mobility of $SrTiO_3$ with strain, Appl. Phys. Lett. 98 (2011), 132102, https://doi.org/10.1063/1.3571447.
[11] J.H. Haeni, P. Irvin, W. Chang, R. Uecker, P. Reiche, Y.L. Li, S. Choudhury, W. Tian, M.E. Hawley, B. Craigo, A.K. Tagantsev, X.Q. Pan, S.K. Streiffer, L.Q. Chen, S. W. Kirchoefer, J. Levy, D.G. Schlom, Room-temperature ferroelectricity in strained $SrTiO_3$, Nature 430 (2004) 758–761, https://doi.org/10.1038/nature02773.
[12] J. Guan, W. Song, L. Yang, D. Tománek, Strain-controlled fundamental gap and structure of bulk black phosphorus, Phys. Rev. B 94 (2016), 045414, https://doi.org/10.1103/PhysRevB.94.045414.
[13] N. Vonrüti, U. Aschauer, Band-gap engineering in $AB(O_xS_{1-x})_3$ perovskite oxysulfides: a route to strongly polar materials for photocatalytic water splitting, J. Mater. Chem. A 7 (2019) 15741–15748, https://doi.org/10.1039/c9ta03116b.
[14] R.U. Chandrasena, W. Yang, Q. Lei, M.U. Delgado-Jaime, K.D. Wijesekara, M. Golalikhani, B.A. Davidson, E. Arenholz, K. Kobayashi, M. Kobata, F.M.F. de Groot, U. Aschauer, N.A. Spaldin, X. Xi, A.X. Gray, Strain-engineered oxygen vacancies in $CaMnO_3$ thin films, Nano Lett. 17 (2017) 794–799, https://doi.org/10.1021/acs.nanolett.6b03986.
[15] Y. Kim, M. Watanabe, J. Matsuda, A. Staykov, H. Kusaba, A. Takagaki, T. Akbay, T. Ishihara, Chemo-mechanical strain effects on band engineering of the TiO_2 photocatalyst for increasing the water splitting activity, J. Mater. Chem. A 8 (2020) 1335–1346, https://doi.org/10.1039/C9TA11048H.
[16] L. Ni, Y. Liu, C. Song, W. Wang, G. Han, Y. Ge, First-principle study of strain-driven phase transition in incipient ferroelectric $SrTiO_3$, Phys. B Condens. Matter 406 (2011) 4145–4149, https://doi.org/10.1016/j.physb.2011.08.018.
[17] A. Herklotz, S.F. Rus, T.Z. Ward, Continuously controlled optical band gap in oxide semiconductor thin films, Nano Lett. 16 (2016) 1782–1786, https://doi.org/10.1021/acs.nanolett.5b04815.
[18] D. Zou, Y. Liu, S. Xie, J. Lin, J. Li, Effect of strain on thermoelectric properties of $SrTiO_3$: first-principles calculations, Chem. Phys. Lett. 586 (2013) 159–163, https://doi.org/10.1016/j.cplett.2013.09.036.
[19] A. Janotti, D. Steiauf, C.G. Van de Walle, Strain effects on the electronic structure of $SrTiO_3$: toward high electron mobilities, Phys. Rev. B 84 (2011), 201304, https://doi.org/10.1103/PhysRevB.84.201304.
[20] Y.J. Chang, G. Khalsa, L. Moreschini, A.L. Walter, A. Bostwick, K. Horn, A. H. MacDonald, E. Rotenberg, Uniaxial strain induced band splitting in semiconducting $SrTiO_3$, Phys. Rev. B 87 (2013), 115212, https://doi.org/10.1103/PhysRevB.87.115212.
[21] Z. Lan, T. Vegge, I.E. Castelli, theoretical insight on anion ordering, strain, and doping engineering of the oxygen evolution reaction in $BaTaO_2N$, Chem. Mater. 33 (2021) 3297–3303, https://doi.org/10.1021/acs.chemmater.1c00370.
[22] Z. Lan, D.R. Småbråten, C. Xiao, T. Vegge, U. Aschauer, I.E. Castelli, Enhancing oxygen evolution reaction activity by using switchable polarization in ferroelectric $InSnO_2N$, ACS Catal. 11 (2021) 12692–12700, https://doi.org/10.1021/acscatal.1c03737.
[23] C. Spezzati, Z. Lan, I.E. Castelli, Dynamic strain and switchable polarization: A pathway to enhance the oxygen evolution reaction on $InSnO_2N$, J. Catal. 413 (2022) 720–727, https://doi.org/10.1016/j.jcat.2022.07.021.
[24] J.O. Island, A. Kuc, E.H. Diependaal, R. Bratschitsch, H.S.J. van der Zant, T. Heine, A. Castellanos-Gomez, Precise and reversible band gap tuning in single-layer $MoSe_2$ by uniaxial strain, Nanoscale 8 (2016) 2589–2593, https://doi.org/10.1039/C5NR08219F.
[25] Y. Li, Z. Hu, S. Lin, S.K. Lai, W. Ji, S.P. Lau, Giant anisotropic raman response of encapsulated ultrathin black phosphorus by uniaxial strain, Adv. Funct. Mater. 27 (2017) 1600986, https://doi.org/10.1002/adfm.201600986.
[26] A.R. Silva, G.M. Dalpian, Vacancies at $LaAlO_3$ thin films: A 2D electron gas at the surface, J. Alloy. Compd. 684 (2016) 544–548, https://doi.org/10.1016/j.jallcom.2016.05.045.
[27] A.R. Silva, G.M. Dalpian, Oxygen vacancies at the surface of $SrTiO_3$ thin films, J. Appl. Phys. 115 (2014), 033710, https://doi.org/10.1063/1.4861730.
[28] Y.L. Li, D.N. Zhang, S.B. Qu, M. Yang, Y.P. Feng, The effect of oxygen vacancies on the electronic structures, magnetic properties and the stability of $SrTiO_3$(001) surface, Surf. Sci. 641 (2015) 37–50, https://doi.org/10.1016/j.susc.2015.04.020.
[29] W. Sitaputra, N. Sivadas, M. Skowronski, D. Xiao, R.M. Feenstra, Oxygen vacancies on SrO-terminated $SrTiO_3$(001) surfaces studied by scanning tunneling spectroscopy, Phys. Rev. B – Condensed Matter Mater. Phys. 91 (2015), https://doi.org/10.1103/PhysRevB.91.205408.
[30] A. Marthinsen, T. Grande, S.M. Selbach, Microscopic Link between Electron Localization and Chemical Expansion in $AMnO_3$ and $ATiO_3$ Perovskites (A = Ca, Sr, Ba), J. Phys. Chem. C 124 (2020) 12922–12932, https://doi.org/10.1021/acs.jpcc.0c02060.
[31] D.S. Aidhy, B. Liu, Y. Zhang, W.J. Weber, Chemical expansion affected oxygen vacancy stability in different oxide structures from first principles calculations, Comput. Mater. Sci 99 (2015) 298–305, https://doi.org/10.1016/j.commatsci.2014.12.030.
[32] I.E. Castelli, T. Olsen, S. Datta, D.D. Landis, S. Dahl, K.S. Thygesen, K.W. Jacobsen, Computational screening of perovskite metal oxides for optimal solar light capture, Energ. Environ. Sci. 5 (2012) 5814–5819, https://doi.org/10.1039/C1EE02717D.

[33] J. Sun, A. Ruzsinszky, J. Perdew, Strongly constrained and appropriately normed semilocal density functional, Phys. Rev. Lett. 115 (2015), 036402, https://doi.org/10.1103/PhysRevLett.115.036402.
[34] G. Kresse, J. Hafner, Ab initio molecular dynamics for liquid metals, Phys. Rev. B 47 (1993) 558–561, https://doi.org/10.1103/PhysRevB.47.558.
[35] V.I. Anisimov, J. Zaanen, O.K. Andersen, Band theory and Mott insulators: Hubbard U instead of Stoner I, Phys. Rev. B 44 (1991) 943–954, https://doi.org/10.1103/PhysRevB.44.943.
[36] M. Kaltak, M. Fernández-Serra, M.S. Hybertsen, Charge localization and ordering in $A_2Mn_8O_{16}$ hollandite group oxides: impact of density functional theory approaches, Phys. Rev. Mater. 1 (2017), https://doi.org/10.1103/PhysRevMaterials.1.075401.
[37] DTU Data repository, https://doi.org/10.11583/DTU.20036264.
[38] L. Cao, E. Sozontov, J. Zegenhagen, Cubic to tetragonal phase transition of $SrTiO_3$ under epitaxial stress: an x-ray backscattering study, Phys. Status Solidi (a). 181 (2000) 387–404, https://doi.org/10.1002/1521-396X(200010)181:2<387::AID-PSSA387>3.0.CO;2-5.
[39] R.A. Evarestov, Theoretical modeling of inorganic nanostructures: Symmetry and ab-initio calculations of nanolayers, nanotubes and nanowires, 2015.
[40] L. Zhang, B. Liu, H. Zhuang, P.R.C. Kent, V.R. Cooper, P. Ganesh, H. Xu, Oxygen vacancy diffusion in bulk $SrTiO_3$ from density functional theory calculations, Comput. Mater. Sci 118 (2016) 309–315, https://doi.org/10.1016/j.commatsci.2016.02.041.